Ordering of hard particles between hard walls

2001 J. Phys.: Condens. Matter 13 4715

(http://iopscience.iop.org/0953-8984/13/21/306)

INSTITUTE OF PHYSICS PUBLISHING JOURNAL OF PHYSICS: CONDENSED MATTER

J. Phys.: Condens. Matter **13** (2001) 4715–4726 www.iop.org/Journals/cm PII: S0953-8984(01)19898-X

Ordering of hard particles between hard walls

A Chrzanowska[1,4], P I C Teixeira[2,5], H Ehrentraut[1] and D J Cleaver[3]

[1] Institut für Mechanik (AG3), Technische Universität Darmstadt, Hochschulstraße 1, D-64289 Darmstadt, Germany
[2] Departamento de Engenharia de Materiais, Instituto Superior Técnico, Avenida Rovisco Pais, P-1049-001 Lisbon, Portugal
[3] Materials Research Institute, Sheffield Hallam University, Pond Street, Sheffield S1 1WB, UK

E-mail: paulo@ist.utl.pt (P I C Teixeira)

Received 8 December 2000, in final form 7 March 2001

Abstract

The structure of a fluid of hard Gaussian overlap particles of elongation $\kappa = 5$, confined between two hard walls, has been calculated from density-functional theory and Monte Carlo simulations. By using the exact expression for the excluded volume kernel (Velasco E and Mederos L 1998 *J. Chem. Phys.* **109** 2361) and solving the appropriate Euler–Lagrange equation entirely numerically, we have been able to extend our theoretical predictions into the nematic phase, which had up till now remained relatively unexplored due to the high computational cost. Simulation reveals a rich adsorption behaviour with increasing bulk density, which is described semi-quantitatively by the theory without any adjustable parameters.

1. Introduction

There are many areas of soft matter in which the shapes of constituent particles are important. These extend across the lengthscales: from molecular liquid crystals (LCs) [1]; to supramolecular aggregates such as certain types of virus [2]; to the new non-spherical colloids that can now be synthesized in a well-controlled manner [3]; and, finally, to biological granular materials such as red blood cells. Of these, LCs are a particularly useful class: being easily oriented by external electric or magnetic fields, or by suitably prepared surfaces, they have found wide application in display devices [4]. Besides their intrinsic interest, models of LCs—or, more generally, of anisotropic fluids—can provide insight into seemingly very different phenomena: indeed, the recent discovery that cell DNA can form a so-called untwisted line hexatic phase [5], originally predicted in a nematic context [6], has definitely established LCs as a living subject.

Although the technological interest of LCs arises from their behaviour in confined geometries, only recently has this become amenable to study. Experimental techniques such as scanning tunnelling microscopy [7], scanning near-field optical microscopy, atomic force

[4] Permanent address: Institute of Physics, Kraków University of Technology, ul. Podchorążych 1, 30-084 Kraków, Poland.
[5] Author for correspondence.

microscopy [8], evanescent wave ellipsometry [9], second harmonic generation [10], or sum-frequency vibrational spectroscopy [11], allow the structure and orientational order of LC films to be resolved on the molecular scale. Finally, the full orientation profiles can be obtained from deuterium nuclear magnetic resonance [12] or, for some geometries, waveguiding techniques [13]. At the same time, thanks to major increases in computer power, we are now able to numerically model fairly realistic inhomogeneous systems on a desktop workstation.

Surface anchoring, as the alignment of an anisotropic fluid by a substrate is known, thus plays a crucial role in the fabrication of most such devices. Although much empirical knowledge exists on how to treat surfaces in order to obtain the desired anchoring properties, our understanding of the underlying physical processes is still very limited. Typically these relate to the interplay between surface and intermolecular interactions, and to the crucial role of density inhomogeneities [14]. In particular, the coupling of density and orientational order can lead to highly non-trivial results such as complex wetting behaviour [15]. *Empirical* rules for predicting the most stable alignment on the basis of the relative magnitudes of the solid-fluid surface tensions for different orientations [16] have met with some success. However, they reveal little of the microscopic intricacies of the phenomenon. Steric considerations, based on the detailed shapes of molecules, have proved effective in explaining some results [17], but are extremely case-specific. Elastic theory has been used to describe LCs at grooved surfaces [18]. Yet it assumes (i) slow spatial variation of the director; (ii) uniaxiality; and (iii) spatial uniformity of the scalar order parameter, which recent experiments [7] and simulations [19] show not to be valid close to a solid substrate. Landau–de Gennes theory [20] removes all of these assumptions, but still neglects density inhomogeneities. Moreover, it introduces phenomenological parameters not easily related to microscopic quantities. Early *microscopic* theories of the solid-nematic interface either assumed the LC to be bulk-like right up to the surface [21, 22], or constrained the density profile to have a special form [23, 24]; more recent work [25–28] has gone beyond this, even considering curved hard surfaces [29].

Here we revisit the basic problem of finding the structure of a fluid of hard rods between two hard (flat and structureless) walls. This is readily identified as the simplest possible model of a confined LC or anisotropic colloidal suspension, but it also relates to granular materials, which can be made to attain entropically-favourable states by means of vibration. (In a hard-core system such as this, the free energy contains only entropic contributions, which nevertheless lead to surprisingly rich behaviour.) Previous work [25, 26] considered only the case where the bulk (i.e. the central part of the film) is isotropic, or where rods are constrained to point along the three coordinate axes (cf. the theory—but not the simulations—of [28]). We have performed the first density-functional calculation of the density and order parameter profiles of moderately-elongated hard rods with continuous orientations, for bulk densities in the nematic range. In addition, we have not assumed any functional forms, or made use of any expansions, either of the interaction kernel or of the distribution functions, but instead fully numerically solved the Euler–Lagrange equation that follows from minimization of the free energy. The only limitation comes from employing the second-virial (Onsager) approximation: Allen [30] has reported excellent agreement between theory and simulation for hard ellipsoids of length-to-breadth ratio $\kappa = 15$, but this is expected to worsen for smaller particle elongations.

This paper is organized as follows: in section 2 we describe our model and the simple Onsager second-virial approximation we used to treat it. Then in section 3 we highlight several novel aspects of the algorithm employed for the solution of the Euler–Lagrange equation, and compare our theoretical predictions for the density and order parameter profiles with Monte Carlo (MC) simulation results. We also assess the validity of an earlier approach by one of us, where the density, order parameter and tilt angle profiles were assumed to be step functions [22]. Finally in section 4 we discuss some directions for future research.

2. Theory

We model the interaction between uniaxial rod-like particles by means of the hard Gaussian overlap (HGO) potential used previously in 3d bulk simulations and Onsager theory of lyotropic LC behaviour [31] (i.e. where the LC phase transitions are driven by density, rather than temperature, changes):

$$U_{12}(\boldsymbol{r}_{12}, \omega_1, \omega_2) = \begin{cases} 0 \text{ if } r_{12} \geqslant \sigma(\hat{\boldsymbol{r}}_{12}, \omega_1, \omega_2) \\ \infty \text{ if } r_{12} < \sigma(\hat{\boldsymbol{r}}_{12}, \omega_1, \omega_2) \end{cases} \tag{1}$$

where $\omega_i = (\theta_i, \phi_i)$ are the polar and azimuthal angles describing the orientation of the long axis of particle i, and and $\hat{\boldsymbol{r}}_{12} = \boldsymbol{r}_{12}/r_{12}$ is a unit vector along the line connecting the centres of the two particles. The range parameter function is given by

$$\sigma(\hat{\boldsymbol{r}}_{12}, \omega_1, \omega_2) = \sigma_0 \left[1 - \frac{1}{2}\chi \left\{ \frac{(\hat{\boldsymbol{r}}_{12} \cdot \hat{\omega}_1 + \hat{\boldsymbol{r}}_{12} \cdot \hat{\omega}_2)^2}{1 + \chi(\hat{\omega}_1 \cdot \hat{\omega}_2)} + \frac{(\hat{\boldsymbol{r}}_{12} \cdot \hat{\omega}_1 - \hat{\boldsymbol{r}}_{12} \cdot \hat{\omega}_2)^2}{1 - \chi(\hat{\omega}_1 \cdot \hat{\omega}_2)} \right\} \right]^{-\frac{1}{2}} \tag{2}$$

where $\hat{\omega}_i = (\cos\phi_i \ \sin\theta_i, \sin\phi_i \ \sin\theta_i, \cos\theta_i)$ and $\chi = (\kappa^2 - 1)/(\kappa^2 + 1)$, κ being the particle length to breadth ratio, σ_L/σ_0. For moderate κ, the HGO model is a good approximation to the hard ellipsoid (HE) contact function [32, 33]; furthermore, their virial coefficients (and thus their equations of state, at least at low to moderate densities) are very similar [34]. Finally, it has the considerable computational advantage over HEs that $\sigma(\hat{\boldsymbol{r}}_{12}, \omega_1, \omega_2)$, the distance of closest approach between two particles, is given in closed form. Particle–substrate interactions have been modelled using a hard needle–wall potential

$$U_{wall}(z, \theta) = \begin{cases} 0 \text{ if } |z - z_0| \geqslant \frac{\sigma_L}{2}\cos\theta \\ \infty \text{ if } |z - z_0| < \frac{\sigma_L}{2}\cos\theta \end{cases} \tag{3}$$

where z_0 represents the location of a substrate. Physically, this corresponds to a system where the molecules are able to embed their side groups into, e.g. an adsorbed surface layer.

In order to find the equilibrium density distribution of a HGO film, we start from the grand-canonical functional [35]

$$\begin{aligned} \beta\Omega[\rho(\boldsymbol{r}, \omega)] &= \beta\mathcal{F}[\rho(\boldsymbol{r}, \omega)] + \beta \int \left[\sum_{i=1}^{2} U_{wall}(\theta, |z - z_0^i|) - \mu \right] \rho(\boldsymbol{r}, \omega) \mathrm{d}\boldsymbol{r}\mathrm{d}\omega \\ &= \int \rho(\boldsymbol{r}, \omega) \left[\log \rho(\boldsymbol{r}, \omega) - 1 \right] \mathrm{d}\boldsymbol{r}\mathrm{d}\omega \\ &\quad - \frac{1}{2} \int \rho(\boldsymbol{r}_1, \omega_1) f_{12}(\boldsymbol{r}_1, \omega_1, \boldsymbol{r}_2, \omega_2) \rho(\boldsymbol{r}_2, \omega_2) \, \mathrm{d}\boldsymbol{r}_1 \mathrm{d}\omega_1 \mathrm{d}\boldsymbol{r}_2 \mathrm{d}\omega_2 \\ &\quad + \beta \int \left[\sum_{i=1}^{2} U_{wall}(|z - z_0^i|, \theta) - \mu \right] \rho(\boldsymbol{r}, \omega) \, \mathrm{d}\boldsymbol{r}\mathrm{d}\omega \end{aligned} \tag{4}$$

where $\mathcal{F}[\rho(\boldsymbol{r}, \omega)]$ is the intrinsic Helmholtz free energy of the inhomogeneous fluid, $f_{12}(\boldsymbol{r}_1, \omega_1, \boldsymbol{r}_2, \omega_2) = \exp[-\beta U_{12}(\boldsymbol{r}_1, \omega_1, \boldsymbol{r}_2, \omega_2)] - 1$ is its Mayer function, μ is the chemical potential, z_0^i ($i = 1, 2$) are the positions of the two substrates, and, because we are dealing with hard-body interactions only, for which the temperature is an irrelevant variable, we can set $\beta = 1/k_{\mathrm{B}}T = 1$ in all practical calculations (we retain it in the formulae for generality). $\rho(\boldsymbol{r}, \omega)$ is the density-orientation profile in the presence of the external potential $U_{wall}(z, \theta)$; it is normalized to the total number of particles N,

$$\int \rho(\boldsymbol{r}, \omega) \, \mathrm{d}\boldsymbol{r}\mathrm{d}\omega = N \tag{5}$$

and is related to the probability that a particle positioned at $\boldsymbol{r}$ has orientation between ω and $\omega + \mathrm{d}\omega$ [6]. Then from equation (1) it follows that the interaction term in equation (4) is just the excluded volume of two HGO particles, weighted by the density-orientation distributions $\rho(\boldsymbol{r}, \omega)$. This equation constitutes the Onsager approximation to the free energy of the confined HGO fluid.

In equation (3) we have implicitly chosen the z-axis to be perpendicular to the walls. We further assume that there is no in-plane structure, so that all quantities are functions of z only. Then equation (4) simplifies to

$$\begin{aligned}\frac{\beta\Omega\left[\rho(z,\omega)\right]}{S_{xy}} &= \int \rho(z,\omega)\left[\log\rho(z,\omega) - 1\right]\mathrm{d}z\mathrm{d}\omega \\ &\quad -\frac{1}{2}\int \rho(z_1,\omega_1)\Xi(z_1,\omega_1,z_2,\omega_2)\rho(z_2,\omega_2)\,\mathrm{d}z_1\mathrm{d}\omega_1\mathrm{d}z_2\mathrm{d}\omega_2 \\ &\quad +\beta\int\left[\sum_{i=1}^{2} U_{wall}(|z - z_0^i|,\theta) - \mu\right]\rho(z,\omega)\,\mathrm{d}z\mathrm{d}\omega \end{aligned} \tag{6}$$

where S_{xy} is the interfacial area. $\Xi(z_1, \omega_1, z_2, \omega_2)$ is now the area of a slice (cut parallel to the bounding plates) of the excluded volume of two HGO particles of orientations ω_1 and ω_2 and centres at z_1 and z_2 [25]; let us call it the *excluded slice*. A major advantage from the computational point of view is that an analytical expression has been derived for the excluded slice of HGO particles [36]. Note that for $|z_i - z_0^i| < \sigma_L/2$, i.e. close to the surfaces, the range of θ_i will depend on z_i, and consequently we will need to evaluate and store $\Xi(z_1, \omega_1, z_2, \omega_2)$ as a function of z_1 and z_2 individually, rather than of $|z_1 - z_2|$ (although $\Xi(z_1, \omega_1, z_2, \omega_2)$ is, of course, translationally invariant). We shall come back to this point below.

Minimization of the grand canonical functional, equation (6),

$$\frac{\delta\Omega\left[\rho(z,\omega)\right]}{\delta\rho(z,\omega)} = 0 \tag{7}$$

yields the Euler–Lagrange equation for the density-orientation profile,

$$\log\rho(z,\omega) = \beta\mu - \int' \Xi(z,\omega,z',\omega')\rho(z',\omega')\,\mathrm{d}z'\mathrm{d}\omega' \tag{8}$$

where the effect of the (hard!) wall potential, given by equation (3), has been incorporated through restriction of the range of integration over θ:

$$\int' \mathrm{d}\omega = \int_0^{2\pi}\mathrm{d}\phi\int_{\theta_m}^{\pi-\theta_m}\sin\theta\,\mathrm{d}\theta = \int_0^{2\pi}\mathrm{d}\phi\int_{-\cos\theta_m}^{\cos\theta_m}\mathrm{d}x \tag{9}$$

with

$$\cos\theta_m = \begin{cases} 1 \text{ if } |z - z_0| \geqslant \frac{\sigma_L}{2} \\ \frac{|z-z_0|}{\sigma_L/2} \text{ if } |z - z_0| < \frac{\sigma_L}{2} \end{cases} \tag{10}$$

z_0 being, we recall, the position of a substrate. It is clear from the structure of equation (8) that μ is the Lagrange multiplier associated with requiring that the mean number of particles in the system be N. It is thus equivalent to fix μ or N (see also discussion in [30]): in what follows we opt for the latter, since it allows closer contact with (*NVT*) simulation.

Once $\rho(\omega, z)$ has been found, we can integrate out the angular dependence to get the density profile,

$$\rho(z) = \int \rho(z,\omega)\,\mathrm{d}\omega \tag{11}$$

[6] It is trivial to introduce, by a simple rescaling, a distribution function normalized to unity, if desired.

and use this result to define the orientational distribution function (ODF) $\hat{f}(z,\omega) = \rho(z,\omega)/\rho(z)$, from which we can calculate the orientational order parameters in the laboratory-fixed frame [37]:

$$\eta(z) = \langle P_2(\cos\theta)\rangle = Q_{zz} \tag{12}$$

$$\varepsilon(z) = \langle \sin 2\theta \ \sin\phi\rangle = \frac{4}{3}Q_{yz} \tag{13}$$

$$\nu(z) = \langle \sin 2\theta \ \cos\phi\rangle = \frac{4}{3}Q_{xz} \tag{14}$$

$$\varsigma(z) = \langle \sin^2\theta \ \cos 2\phi\rangle = \frac{2}{3}(Q_{xx} - Q_{yy}) \tag{15}$$

$$\tau(z) = \langle \sin^2\theta \ \sin 2\phi\rangle = \frac{4}{3}Q_{xy} \tag{16}$$

where $\langle\mathcal{A}\rangle = \int \mathcal{A}\hat{f}(z,\omega)\,\mathrm{d}\omega$. These are the five independent components of the nematic order parameter tensor, $Q_{\alpha\beta} = \langle\frac{1}{2}(3\hat{\omega}_\alpha\hat{\omega}_\beta - \delta_{\alpha\beta})\rangle$. In the particular case where there is no twist, i.e. the director is confined to a plane that we can take as the xz plane, $\varepsilon(z) = \tau(z) = 0$.

In earlier work [37, 38], the functional minimization was performed in two stages, i.e. with respect to the ODF and the density profile separately. This is entirely equivalent to direct minimization with respect to $\rho(z,\omega)$, but less convenient for practical purposes when, as in the model considered here (as well as in [25, 26]), there is strong coupling between positional and orientational degrees of freedom coming from a non-spherical particle shape. In the next section we give details of the numerical method employed to solve equation (8).

3. Results

In this section we find the structure of a confined HGO fluid from theory, and validate this by comparison with computer simulation. It is important to realize, however, that owing to the second-virial approximation, the location of the isotropic–nematic (I–N) transition may not be predicted very accurately. Therefore we start by calculating the bulk phase diagram. From the bulk version of equation (6) (i.e. with all spatial integrations extended to $\pm\infty$ and $U_{wall}(z,\theta) = 0$) we have found the pressure and chemical potential of the I and N phases and performed the standard common-tangent construction. Both the angle-averaged second virial coefficient (for the I phase) and the angle-dependent excluded volume (for the N phase) are known analytically (see, e.g. [39]). The remaining integrations over ω_i were carried out by 16-point Gauss–Legendre quadrature.

Figure 1 shows the phase diagram, in terms of the reduced density, $\rho^* = \rho\sigma_0^3$, versus elongation κ; we have also included I–N coexistence points as determined by constant NpT simulation [31]. Not unexpectedly, theory overestimates the coexistence densities and the first-orderness of the transition considerably, with better agreement for the larger κ; for small elongations, the contribution of higher virial coefficients is substantial. Ginzburg *et al* [40] obtained an even stronger transition and a stronger dependence of the coexistence curves on κ, but this may be a numerical artifact: in our experience, it is crucial to use a large number of integration points and impose a stringent convergence condition. More sophisticated theories [41,42] have been applied to the I–N transition of hard rods; in particular, Parsons–Lee rescaling [42] has been shown to yield very good agreement with simulation [43]. However, their extension to non-uniform systems is highly non-trivial [44]. In this paper we seek to establish how useful the simpler Onsager approximation is for describing ultra-thin (a few molecular lengths) films of moderately elongated particles. All results presented henceforth are for $\kappa = 5$, with the distance between bounding walls fixed at $L = 20\sigma_0$.

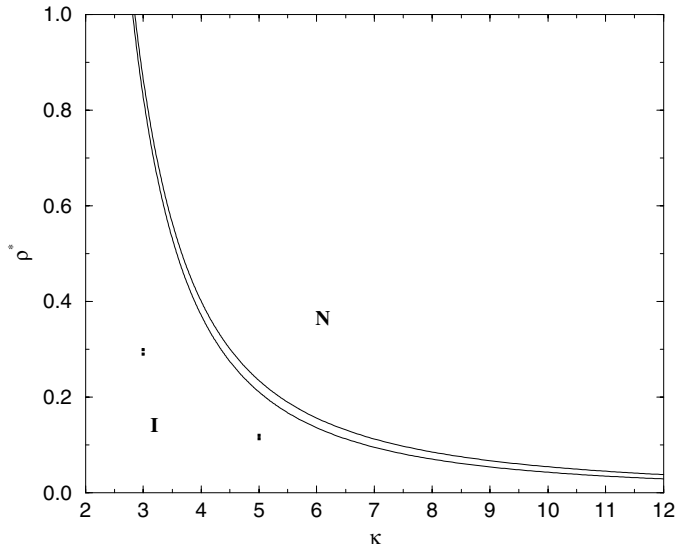

Figure 1. N–I phase transition of the HGO fluid, from theory. $\rho^* = \rho\sigma_0^3$ and κ are the reduced density and the elongation, respectively. The symbols (filled squares) are simulation results from [31].

Equation (8) was solved iteratively by the Picard method, with an admixture parameter of 0.9 (i.e. 90% of 'old' solution in each iteration), starting from a uniform and isotropic profile. Integrations were performed by Gauss–Legendre quadrature, using 64 z-points (the minimum necessary to resolve the structure of profiles at the higher densities considered) and 16×16 ω-points (for consistency with the bulk calculation). Note that the range of ω' depends on z': the closer a particle is to a substrate, the fewer orientations are accessible. In order to achieve good accuracy it is nevertheless crucial to include the same number of points in the angular integrations for all z'. Results were collected after 600 iterations, which is dictated by the computational cost. Convergence errors, defined as the sum of the absolute values of differences between consecutive iterates at $64 \times 16 \times 16 = 16\,384$ points, varied between 10^{-1} and 10^{-8}, depending on the bulk density.

For comparison, we have also simulated a system of 1000 HGO particles using Metropolis Monte Carlo (MC) in the canonical (*NVT*) ensemble. With the substrate separation fixed at $L = 20\sigma_0$, the two remaining box dimensions were set equal to each other at values appropriate to each required density. Simulations were performed in a compression sequence starting at $\rho^* = 0.08$, each run being initiated from a compressed version of a configuration previously equilibrated at a neighbouring density. To avoid overlaps in these initial configurations, compressions were effected via a series of intermediate steps, overlaps being checked for and removed (using particle displacement moves) at each step. Production run lengths at each density investigated were set at 2.5×10^5 MC sweeps (where one sweep comprises one attempted move per particle), equilibration requiring between 2.5×10^5 and 10^6 MC sweeps. Maximum translational and rotational move parameters were allowed to vary during the equilibration stage until they yielded acceptance ratios of approximately 50%. During the production stage, profiles of number density $\rho(z)$, and nematic order parameter, $\eta(z)$, were calculated by dividing the system into 100 equal slices aligned parallel to the confining walls.

As noted above in connection with figure 1, the I–N transition occurs at different densities,

and with different widths, in theory and in simulation. The question then arises of how to meaningfully compare theory and simulation results. Allen and co-workers [45] proposed a phenomenological scaling of the density profile at the I–N interface that seems very well suited for this purpose: $d(z) \equiv (\rho(z) - \rho_I)/(\rho_N - \rho_I)$ from theory and simulation were in very satisfactory agreement. Here we extend Allen *et al*'s approach and choose state points characterised by the same $d_{bulk} \equiv (\rho_{bulk} - \rho_I)/(\rho_N - \rho_I)$. Of course, it is essential to have accurate I–N coexistence densities. From theory, $\rho_I^{*,th} = 0.2107$ and $\rho_N^{*,th} = 0.2347$; whereas from MC NpT simulation of a 256-particle system Padilla and Velasco [31] found $\rho_I^{*,sim} \simeq 0.113$ and $\rho_N^{*,sim} \simeq 0.12$. Noting Padilla and Velasco's statement that due to the small number of particles used "the accuracy of these estimates is uncertain", in this work we have taken $\rho_I^{*,sim} = 0.116$ since this improves the accord between theoretical and simulated order parameters (see below). At this stage, we cannot determine whether this slight adjustment is needed simply because of a possible error in Padilla and Velasco's $\rho_I^{*,sim}$ or whether it is due to the slight upward shift of $\rho^{*,th}$ of the confined film relative to the bulk[7]. This matter will likely only be resolved by locating the I–N transition of the (bulk as well as confined) HGO fluid in a more precise MC study. Still, we regard Allen *et al*'s scaling as the best working tool for comparison of these systems, despite the fact that it lacks a more fundamental justification. The unscaled densities at which simulation runs and theory calculations have been performed, as well as the symbols used in figures 2–4, are collected in table 1.

Table 1. Scaled densities d_{bulk} for comparison of theory (th) and simulation (sim) results. $\rho^{*,th}$ and $\rho^{*,sim}$ are the unscaled densities at which the theoretical calculations and the simulations have been performed. Also included are the symbols/line styles corrsponding to each d_{bulk} in figures 2–4.

d_{bulk}	$\rho^{*,th}$	Line style(th)	$\rho^{*,sim}$	Symbol (sim)
−0.25	0.2047	Solid	0.115	Circles
1.00	0.2347	Long-dashed	0.12	Squares
2.25	0.2647	Short-dashed	0.125	Diamonds
3.50	0.2947	Dot-dashed	0.13	Right triangles

In figure 2 we plot representative $d(z)$ profiles (only two for clarity) corresponding to bulk densities in the high-density isotropic and and well-developed nematic regions (other authors [21,25,26] have previously addressed the low-density regime). Characteristically, the density is not uniform and there is marked equilibrium peak formation. This feature is captured by both simulation and theory, although the latter underestimates, sometimes severely, the height of the peaks and the depth of the troughs. Recall that at lower densities, in the isotropic bulk range, the density profile of hard rods of *finite* elongation exhibits two peaks: one, at $|z - z_0| \simeq \sigma_L/2$, corresponds to particles able to rotate in 3d without direct interaction with the substrate [46] whilst that at $|z - z_0| \sim 0$ corresponds to particles lying approximately parallel with the substrate. In the higher-density situations considered here, the surface peaks dominate, and further peaks begin to form farther into the bulk, suggesting that the dominant mechanism is now layering. This interpretation is supported by experimental evidence [47].

Figure 3 shows the density-driven evolution of the order parameter profile $\eta(z) = Q_{zz}(z)$. In the isotropic phase, $Q_{zz}(z)$ is everywhere zero except in the surface layers, by which we understand the regions in which the rotational freedom of a particle is restricted by the presence of the walls. Because the walls are impenetrable, see equation (3), the thickness of these layers is half the length of a particle, $2.5\sigma_0$. The consequence of this hindrance at the walls is then

[7] In a layer as thin as this, the I–N transition will be slightly shifted in density relative to the bulk, see [28]. We have not investigated this in detail.

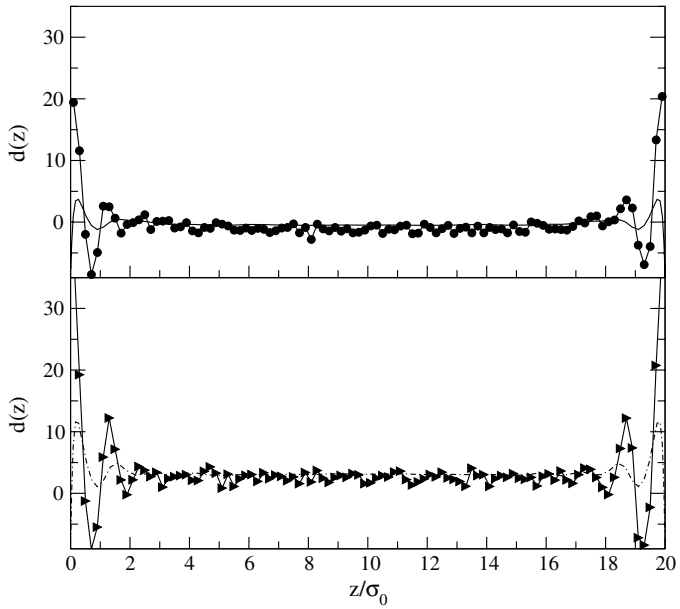

Figure 2. Scaled density $d(z)$ for $d_{bulk} = -0.25$ (top, I range) and $d_{bulk} = 3.50$ (bottom, N range). Symbols are from simulation, solid (top) and dot-dashed (bottom) lines are from theory (the lines connecting the simulation data points are just to guide the eye). See text and table 1 for details.

nematic order with symmetry axis along the z-direction, around which particles are distributed isotropically but with polar angles on average greater than 45 degrees ('antinematic', as in [28]). This yields $Q_{zz}(z) < 0$ in the surface layers, with the expected limit of -0.5 at the walls (it is quadratic in z in the limit of very low densities) [21]. On increasing the density a transition takes place into an anisotropic phase, later to be recognized as a uniaxial nematic, at which $Q_{zz}(z)$ becomes finite throughout the film. Because of the walls, the change from I to N is not uniform in the bulk beyond the surface layers: rather, the N phase grows inwards from the substrates, as seen in [28]. Immediately after the transition the $Q_{zz}(z)$ profile retains its parabolic shape at the walls [21], but at higher densities it becomes flat again (but now non-zero everywhere), with a degree of order more or less uniform. A tendency is then also observed to mirror the peak structure of the density profiles, but this is not very pronounced.

$Q_{xx}(z)$ is plotted in figure 4. This is positive at the walls and vanishes in the bulk when the overall density pertains to the isotropic phase (the simulation results remain at $\simeq 0.25$ due to finite-size effects). At the transition point the bulk value rises is a manner similar to $Q_{zz}(z)$, i.e. it is seeded at the walls. As will become apparent from figure 5, Q_{xx} plays the role of the main uniaxial order parameter.

In figure 5 the three diagonal components, $Q_{xx}(z)$, $Q_{yy}(z)$ and $Q_{zz}(z)$, of the order parameter tensor, calculated from theory at three different densities: $\rho^{*,th} = 0.16$, 0.19 and 0.25 can be seen. Analysis of all three is indispensable for phase identification. The off-diagonal components vanish at all densities, implying absence of twist in the structure. For $\rho^* = 0.16$ the three diagonal order parameters are zero save in the surface layers. $Q_{zz}(z)$ attains -0.5 at $z = 0$ and $z = L$, which indicates, unsurprisingly, perfect order parallel to the substrates. In addition, the whole film is uniaxial: $Q_{xx}(z) = Q_{yy}(z)$, taking the value 0.25 at the walls. Traditionally in LCs the director is taken to be given by the eigenvector associated with the largest eigenvalue of $\boldsymbol{Q}$. Here we cannot talk of a director (a mesoscopic

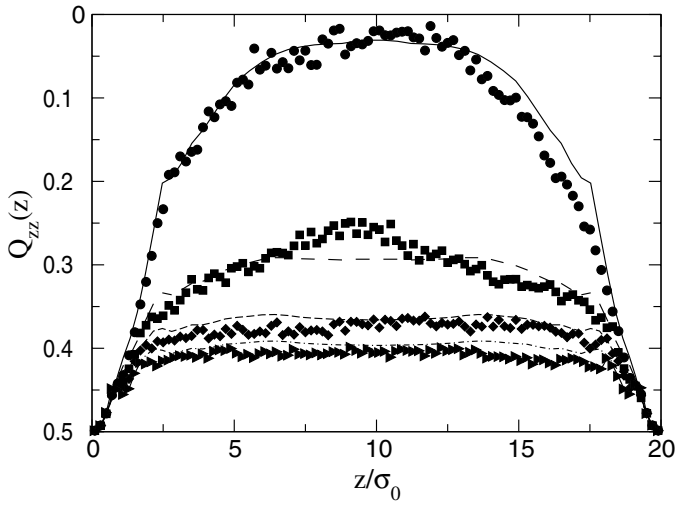

Figure 3. Order parameter $Q_{zz}(z) \equiv \eta(z)$ measured along the normal to the substrates. Symbols are simulation points, lines are from theory. See table 1 for details.

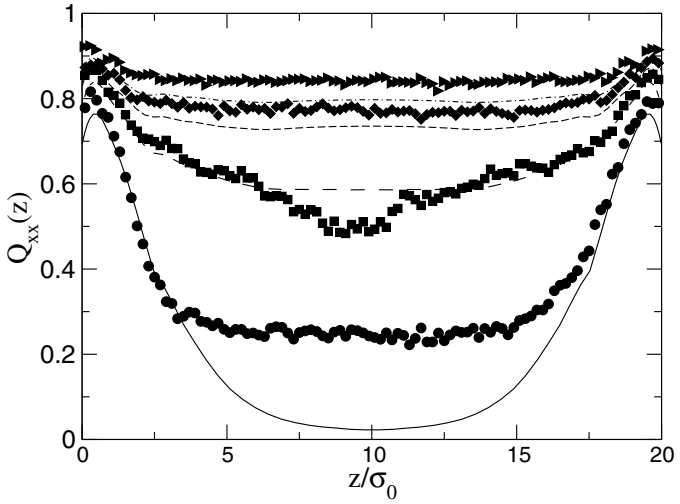

Figure 4. Order parameter $Q_{xx}(z)$. Symbols as in figure 3.

entity) since no appropriate coarse graining is involved. Instead we utilize the concept of a symmetry axis. In the present case this is associated with the lowest eigenvalue, which is the largest in absolute value. As the density is increased, the ordered surface layers remain unchanged until they undergo a uniaxial-to-biaxial transition, as follows from the fact that at $\rho^* = 0.19$, $Q_{xx}(z) \neq Q_{yy}(z)$ Although the surface regions are now biaxial, the bulk remains isotropic. No sharp isotropic-biaxial nematic interface is seen, but rather an interfacial region of thickness about half a particle length. The observation of a surface biaxial phase at a density lower than that of the bulk I–N transition confirms earlier conclusions derived by Sluckin and Poniewierski [48] and Poniewierski [25] on the basis of Landau–de Gennes theory, as well as the density-functional and simulation results of Van Roij *et al* for hard spherocylinders [28]. Consistently, $Q_{zz}(z)$ is negative at the walls, which is the only possible

outcome in the case of uniaxial hard bodies. Finally, for $\rho^* = 0.25$ a well-developed uniaxial N phase is observed in the central part of the film and there persists biaxial order in the surface regions. However, unlike at lower densities, where it was found that $Q_{xx}(z) = Q_{yy}(z)$, we now have $Q_{zz}(z) = Q_{yy}(z)$: the main symmetry axis switched from z to x at the uniaxial-to-biaxial transition. This phenomenon, which in Landau–de Gennes theory is called eigenvalue exchange, does not involve either deformation or *physical* reorientation of the particles. Such a biaxiality-mediated symmetry axis change has also been predicted to occur in the context of hybrid-aligned LC films [49]. More work is needed to establish the order of this transition.

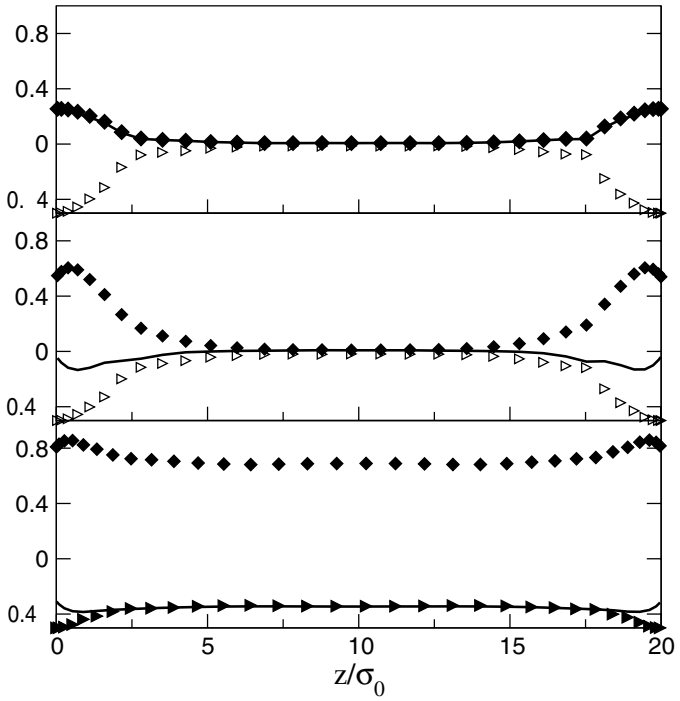

Figure 5. Diagonal components $Q_{xx}(z)$ (diamonds), $Q_{yy}(z)$ (solid line) and $Q_{zz}(z)$ (triangles) of the order parameter tensor $\boldsymbol{Q}$, for $\rho^{*,th} = 0.16$ (top), 0.19 (middle) and 0.25 (bottom). See the text for discussion of the eigenvalue identity exchange phenomenon.

In conclusion, there is good agreement between theory and simulation results for the diagonal components of the order parameter tensor, both in the I and N phases, provided comparison is made at the same scaled density d_{bulk}, defined according to the prescription of Allen *et al*. That the density profiles are much less faithfully reproduced, is hardly surprising, since the Onsager approximation does not yield the correct functional dependence of the order parameters on density. It should be stressed that our method is particularly useful for the nematic phase since it does not require *a priori* knowledge of the chemical potentials: instead, it uses the bulk density as input.

4. Conclusions

In this paper we have presented a density-functional treatment of a HGO fluid confined between parallel hard walls. Despite the simplicity (one might almost say naivety) of the Onsager approximation, we have been able to reproduce qualitatively the density and orientational

structure, as obtained from computer simulation, of particles of elongation $\kappa = 5$. Contrary to what was assumed in earlier work [22], the density-orientation profile is very non-uniform close to the substrates; such inhomogeneity can have dramatic consequences, such as discontinuous orientational transitions [46].

In effecting comparison between theory and simulation, account has to be taken of the fact that they yield rather different I–N transition densities and widths. This is due to our neglect of correlations of order higher than second-virial, which are relevant in the range of densities of interest. Greater predictive power would require a far more sophisticated treatment, such as a weighted-density approximation along the lines of [44]. The development and implementation of such a scheme are, however, highly non-trivial. In keeping with our aim of assessing the validity and usefulness of the Onsager approach, we instead adapted a phenomenological scaling of the density first proposed by Allen and collaborators [45]. Unsurprisingly, agreement is less good than for HEs of ellongation $\kappa = 15$ [30], but its quality is strongly dependent on the accuracy of the isotropic and nematic coexistence densities as determined independently by constant MC NpT simulation. We are currently extending our calculations to other (smaller) particle elongations, including oblate shapes ($\kappa < 1$).

The present theory can be straightforwardly generalized to more sophisticated surface interactions, such as hybrid geometries where different anchorings are favoured at either substrate. This work is in progress and will be reported elsewhere. Finally, though decidedly different in character the basic entropy-driven features of granular systems should be the same; whether and how they can be overcome by dissipation-frictional processes is a challenge for future investigation.

Acknowledgements

We are grateful to R Evans, H N W Lekkerkerker, R J F Leote de Carvalho, F Schmid, M M Telo da Gama and E Velasco for stimulating discussions and suggestions, to H Yokoyama for a very helpful introduction to experimental LC surface techniques, and to C M Care and T J Sluckin for a critical reading of the manuscript. A Chrzanowska acknowledges financial support from Sonderforschungsbereich 298, B13. P I C Teixeira would like to thank the Centro de Física da Matéria Condensada da Universidade de Lisboa for the use of their computing facilities.

References

[1] de Gennes P G and Prost J 1992 *The Physics of Liquid Crystals* 2nd edn. (Oxford: Oxford University Press)
[2] Bawden F C, Pirie N W, Bernal J D and Fankuchen I 1936 *Nature* **138** 1051
[3] Lekkerkerker H N W, Buining P A, Buitenhuis J, Vroege G J and Stroobants A 1995 *Observation, Prediction and Simulation of Phase Transitions in Complex Fluids* ed. M Baus, L F Rull and J-P Ryckaert (Dordrecht: Kluwer)
Ho C C, Ottewill R H and Yu L 1997 *Langmuir* **13** 1925
Jiang P, Bartone J F and Colvin V L 2001 *Science* **291** 453
[4] Schadt M 1993 *Liq. Cryst.* **14** 73
Booth C and Raynes P 1997 *Physics World* **10** 33
[5] Strey H H, Wang J, Podgornik R, Rupprecht A, Yu L, Parseguian V A and Sirota E B 2000 *Phys. Rev. Lett.* **84** 3105
[6] Toner J 1983 *Phys. Rev.* A **27** 1157
[7] Frommer J 1992 *Angew. Chem. Int. Ed. Engl.* **31** 1298
[8] Williamson R L, Rivera M, Miles M J and Jandt K D 1995 SPIE Proceedings **2384** 67
[9] Hsiung H, Rasing T and Shen Y R 1986 *Phys. Rev. Lett.* **57** 3065
[10] Shen Y R 1994 *Appl. Phys.* A *Mater.* **59** 541

[11] Miranda P B and Shen Y R 1999 *J. Phys. Chem.* B **103** 3292
[12] Luckhurst G R, Le Masurier P J, Miyamoto T, Nakamura K, Payne T H, Sugimura A and Timini B A 1997 *Proc. 4th Int. Display Workshop* (Nagoya, Japan) p 65
[13] Yang F Z and Sambles J R 1999 *J. Opt. Soc. Am.* B **16** 488
[14] Jérôme B 1991 *Rep. Prog. Phys.* **54** 391
[15] See, e.g. Sluckin T J and Poniewierski A 1986 *Fluid Interfacial Phenomena* ed. C A Croxton (UK: Wiley)
[16] Creagh L T and Kmetz A R 1973 *Molec. Cryst. Liq. Cryst.* **24** 59
[17] See, e.g. Hiltrop K and Stegemeyer H 1978 *Molec. Cryst. Liq. Cryst.* **49** 61
[18] Berreman D W 1972 *Phys. Rev. Lett.* **28** 1683
[19] Wall G D and Cleaver D J 1997 *Phys. Rev.* E **56** 4306
[20] de Gennes P G 1971 *Molec. Cryst. Liq. Cryst.* **12** 193
Sheng P 1976 *Phys. Rev. Lett.* **37** 1059
Poniewierski A and Sluckin T J 1984 *Molec. Cryst. Liq. Cryst.* **111** 373
Sen A K and Sullivan D E 1987 *Phys. Rev.* A **35** 1391
[21] Hołyst R and Poniewierski A 1988 *Molec. Phys.* **65** 1081
[22] Teixeira P I C and Sluckin T J 1992 *J. Chem. Phys.* **97** 1498
[23] Poniewierski A and Hołyst R 1988 *Phys. Rev.* A **38** 3721
[24] Sharlow M F and Gelbart W M 1992 *Liq. Cryst.* **11** 25
[25] Poniewierski A 1993 *Phys. Rev.* E **47** 3396
[26] Mao Y, Bladon P, Lekkerkerker H N W and Cates M E 1997 *Molec. Phys.* **92** 151
[27] Rodríguez-Ponce I, Romero-Enrique J M, Velasco E, Mederos L and Rull L F 1999 *Phys. Rev. Lett.* **82** 2697
Rodríguez-Ponce I, Romero-Enrique J M, Velasco E, Mederos L and Rull L F 2000 *J. Phys.: Condens. Matter* **12** 363
[28] van Roij R, Dijkstra M and Evans R 2000 *Europhys. Lett.* **49** 350
van Roij R, Dijkstra M and Evans R 2000 *J. Chem. Phys.* **113** 7689
[29] Groh B and Dietrich S 1999 *Phys. Rev.* E **59** 4216
Groh B 1999 *Phys. Rev.* E **59** 5606
[30] Allen M P 1999 *Molec. Phys.* **96** 1391
Allen M P 2000 *J. Chem. Phys.* **112** 5447
[31] Padilla P and Velasco E 1997 *J. Chem. Phys.* **106** 10299
[32] Perram J W and Wertheim M S 1985 *J. Comput. Phys.* **58** 409
Perram J W, Rasmussen J, Praestgaard E and Lebowitz J L 1996 *Phys. Rev.* E **54** 6565
[33] Allen M P, Evans G T, Frenkel D and Mulder B M 1993 *Adv. Chem. Phys.* **86** 1
[34] Bhethanabotla V R and Steele W 1987 *Molec. Phys.* **60** 249
[35] Evans R 1979 *Adv. Phys.* **28** 143
[36] Velasco E and Mederos L 1998 *J. Chem. Phys.* **109** 2361
[37] Telo da Gama M M 1984 *Molec. Phys.* **52** 585
Telo da Gama M M 1984 *Molec. Phys.* **52** 611
[38] Teixeira P I C 1997 *Phys. Rev.* E **55** 2876
[39] Velasco E, Somoza A M and Mederos L 1995 *J. Chem. Phys.* **102** 8107
[40] Ginzburg V V, Glaser M A and Clark N A 1996 *Liq. Cryst.* **21** 265
[41] Mulder B M and Frenkel D 1985 *Molec. Phys.* **55** 1193
[42] Parsons J D 1979 *Phys. Rev.* A **19** 1225
Lee S-D 1987 *J. Chem. Phys.* **78** 4972
[43] McGrother S C, Williamson D C and Jackson G 1996 *J. Chem. Phys.* **104** 6755
Camp P J, Mason C P, Allen M P, Khare A A and Kofke D A 1996 *J. Chem. Phys.* **105** 2837
[44] Somoza A M and Tarazona P 1989 *J. Chem. Phys.* **91** 517
Velasco E, Mederos L and Sullivan D E 2000 *Phys. Rev.* E **62** 3708
[45] McDonald A J, Allen M P and Schmid F 2001 *Phys. Rev.* E **63** 010 701(R)
[46] Cleaver D J and Teixeira P I C 2001 *Chem. Phys. Lett.* at press
[47] Horne R G, Israelachvili J N and Perez E 1981 *J. Physique* **42** 39
[48] Sluckin T J and Poniewierski A 1985 *Phys. Rev. Lett.* **55** 2907
[49] Palffy-Muhoray P, Kelly J R and Gartland E C 1994 *Liq. Cryst.* **16** 713